Larimer, F. W., Lee, E. H., Mural, R. J., Soper, S. T., & Hartman, F. C. (1987) *J. Biol. Chem. 262*, 15327-15329.
Lee, B., & Tabita, F. R. (1990) *Biochemistry 29*, 9352-9357.
Lee, B., Berkas, R. M., & Tabita, F. R. (1991) *J. Biol. Chem. 266*, 7417-7422.
Lee, E. H., Soper, T. S., Mural, R. J., Stringer, C. D., & Hartman, F. C. (1987) *Biochemistry 26*, 4599-4604.
Martin, P. G. (1979) *Aust. J. Plant Physiol. 6*, 401-408.
Mazur, B. J., & Chui, C.-F. (1985) *Nucleic Acids Res. 13*, 2373-2386.
McFadden, B. A., & Small, C. L. (1988) *Photosynth. Res. 18*, 245-260.
Messing, J. (1983) *Methods Enzymol. 101*, 20-78.
Miziorko, H. M. (1979) *J. Biol. Chem. 254*, 270-272.
Morell, M. K., Kane, H. J., & Andrews, T. J. (1990) *FEBS Lett. 265*, 41-45.
Nierzwicki-Bauer, S. A., Curtis, S. E., & Haselkorn, R. (1984) *Proc. Natl. Acad. Sci. U.S.A. 81*, 5961-5965.
Pierce, J., Tolbert, N. E., & Barker, R. (1980) *Biochemistry 19*, 934-942.
Sailland, A., Amiri, I., & Freyssinet, G. (1986) *Plant Mol. Biol. 7*, 213-218.
Sanger, F., Nicklen, S., & Coulson, A. R. (1977) *Proc. Natl. Acad. Sci. U.S.A. 74*, 5463-5467.
Schloss, J. V., Phares, E. F., Long, M. V., Norton, L. I., Stringer, C. D., & Hartman, F. C. (1982) *Methods Enzymol. 90*, 522-528.
Schneider, G., Knight, S., Andersson, I., Brändén, C.-I., Lindqvist, Y., & Lundqvist, T. (1990) *EMBO J. 9*, 2045-2050.
Schneider, S. U., Leible, M. B., & Yang, X.-P. (1989) *Mol. Gen. Genet. 218*, 445-452.
Shinozaki, K., & Sugiura, M. (1983) *Nucleic Acids Res. 11*, 6957-6964.
Smith, D. B., & Johnson, K. S. (1988) *Gene 67*, 31-40.
Starnes, S. M., Lambert, D. H., Maxwell, E. S., Stevens, S. E., Porter, R. D., & Shively, J. M. (1985) *FEMS Microbiol. Lett. 28*, 165-169.
Stiekema, W. J., Wimpee, C. F., & Tobin, E. M. (1983) *Nucleic Acids Res. 11*, 8051-8061.
Tabita, F. R., & Small, C. L. (1985) *Proc. Natl. Acad. Sci. U.S.A. 82*, 6100-6103.
Taylor, J. W., Ott, J., & Eckstein, F. (1985) *Nucleic Acids Res. 13*, 8764-8785.
Terzaghi, B. E., Laing, W. A., Christeller, J. T., Petersen, G. B., & Hill, D. F. (1986) *Biochem. J. 235*, 839-846.
Valentin, K., & Zetsche, K. (1989) *Curr. Genet. 16*, 203-209.
Viale, A. M., Kobayashi, H., & Akazawa, T. (1989) *J. Bacteriol. 171*, 2391-2400.
Voordouw, G., de Vries, P. A., van den Berg, W. A. M., & de Clerk, E. P. J. (1987) *Eur. J. Biochem. 163*, 591-598.
Wagner, S. J., Stevens, S. E., Jr., Nixon, B. T., Lambert, D. H., Quivey, R. G., Jr., & Tabita, F. R. (1988) *FEMS Microbiol. Lett. 55*, 217-222.

Diastereotopic Covalent Binding of the Natural Inhibitor Leupeptin to Trypsin: Detection of Two Interconverting Hemiacetals by Solution and Solid-State NMR Spectroscopy†

Claudio Ortiz, Charles Tellier,‡ Howard Williams, Neal J. Stolowich, and A. Ian Scott*
Center for Biological NMR, Department of Chemistry, Texas A&M University, College Station, Texas 77843-3255
Received January 24, 1991; Revised Manuscript Received July 3, 1991

ABSTRACT: The naturally occurring peptidyl protease inhibitor leupeptin (*N*-acetyl-L-leucyl-L-leucyl-L-argininal) has been prepared labeled with ^{13}C at the argininal carbonyl. ^{13}C chemical shift data for the trypsin–leupeptin inhibitor complex in the pH range 3.0–7.6 reveal the presence of two pH-dependent covalent complexes, suggestive of two interconverting diastereomers at the new asymmetric tetrahedral center created by covalent addition of Ser195 to either side of the ^{13}C-enriched aldehyde of the inhibitor. At pH 7 two signals are observable at δ 98.8 and δ 97.2 (84:16 ratio), while at pH 3.0 the latter signal predominates. In the selective proton ^{13}C-edited NOE spectrum of the major diastereomer at pH 7.4, a strong NOE is observed between the hemiacetal proton of the inhibitor and the C2 proton of His57 of the enzyme, thus defining the stereochemistry of the high pH complex to the *S* configuration in which the hemiacetal oxygen resides in the oxyanion hole. pH titration studies further indicate that the ^{13}C chemical shift of the *S* diastereomer follows a titration curve with a pK_a of 4.69, the magnitude of which is consistent with direct titration of the hemiacetal oxygen. Similar pH-dependent chemical shifts were obtained by using CPMAS ^{13}C NMR, providing evidence for the existence of the same diastereomeric equilibrium in the solid state.

Peptide aldehydes are known to be efficient reversible inhibitors of serine proteases (Thompson, 1973). It has been suggested that the tight binding of the aldehyde results in the formation of a covalent complex between the nucleophilic hydroxyl of the serine protease and the aldehyde carbonyl. One such inhibitor is the slow-binding natural aldehyde leupeptin (*N*-acetyl-L-leucyl-L-leucyl-L-argininal), which reacts with the active site serine (Ser195-OH) of trypsin by a two-step mechanism beginning with formation of a weakly bound complex (K_i = 1.2 mM) followed by covalent bonding (K_d = 1.3 nM) (Aoyagi et al., 1969; Kuramochi et al., 1979). Since the resultant tetrahedral hemiacetal represents a transition

† This research was supported by grants from the National Institutes of Health (GM32596) and the Robert A. Welch Foundation (A-943). C.T., on leave from University of Nantes, acknowledges financial support from NATO.
* To whom correspondence should be addressed.
‡ Present address: Laboratoire de RMN, Faculté des Sciences, University of Nantes, 2 rue de la Houssinière, 44072 Nantes Cedex 03, France.

0006-2960/91/0430-10026$02.50/0

state analogue of peptide hydrolysis, rigorous definition of the structure of the complex would provide stereochemical information important in the understanding of the catalytic mechanism. Furthermore, as enzymes are supposed to bind the transition state more tightly than the substrate (Pauling, 1946), structural studies of these transition state analogue complexes should provide some insight of how serine proteases stabilize the tetrahedral intermediate at the active site.

^{1}H nuclear magnetic resonance (NMR)[1] spectroscopy has provided indirect evidence that specific aldehyde inhibitors form stable hemiacetals with serine proteases (Chen et al., 1979), while ^{19}F and ^{13}C NMR spectroscopy has enabled direct observation of both hemiketals (Malthouse et al., 1985; Liang & Abeles, 1987) and hemiacetals (Shah & Gorenstein, 1983; Shah et al., 1984) with trypsin and chymotrypsin when these enzymes are inhibited with site-specific carbonyl reagents. Although such NMR studies have allowed direct pH titration of the tetrahedral complexes (Malthouse et al., 1985; Liang & Abeles, 1987) contradictory conclusions have been reached concerning the ionization state of the tetrahedral adduct and the active site residues as a function of pH (Kennedy & Schultz, 1979; Brady et al., 1989). Additionally, two pH-dependent tetrahedral forms have been observed in the *N*-acetyl-L-phenylalaninal–chymotrypsin complex (Shah et al., 1984) by ^{13}C NMR. However, the firm assignment of the observed signals, either to different conformers or to diastereomers, could not be made without further experimental data on the environment of the tetrahedral adduct.

In the present study, we provide direct ^{13}C NMR evidence for the formation of two pH-dependent tetrahedral complexes between [1-^{13}C]leupeptin and trypsin. To examine further the structure of these tetrahedral adducts, we have used selective ^{1}H-edited heteronuclear 1D NOESY techniques (Griffey & Redfield, 1987; Tellier et al., 1990). This new active site mapping method has allowed us to define the immediate environment of the hemiacetal proton and demonstrate that, at neutral pH, the bound tetrahedral leupeptin complex exists primarily in the *S* configuration with the oxyanion of the hemiacetal pointed toward the oxyanion hole in the active site.

Materials and Methods

Materials. Trypsin (type III-S, twice crystallized, salt free, from bovine pancreas) was obtained from Sigma Chemical Co. and consisted of 75% β-trypsin and 25% α-trypsin on the basis of chromatographic analysis. As the ^{13}C NMR signals corresponding to the formation of the hemiacetal complex with leupeptin are identical when either pure β-trypsin or the commercial preparation is used; the latter (lot 34F-8140) was used without further purification.

*Synthesis of N-Acetyl-*L*-leucyl-*L*-leucyl-*L*-[1-^{13}C]argininal ([^{13}C]Leupeptin).* Leupeptin was synthesized essentially by the method of Borin et al. (1981), coupling the hydroxysuccimide ester of *N*-acetyl-Leu-Leu with CBZ-arginyl lactam, the latter compound prepared from the appropriately labeled L-[1-^{13}C]arginine-HCl (250 mg) by using the modification of Bajusz et al. (1986) to give [1-^{13}C]leupeptin (99 mg) in 27% overall yield. Full synthetic and spectroscopic details are described elsewhere (Ortiz, 1990).

Inhibition of Trypsin by [^{13}C]Leupeptin. Trypsin (25 mg) was added to a solution of [1-^{13}C]leupeptin (2 equiv) at pH 7.4 in 0.1 M phosphate buffer and allowed to react for 2 h at 4 °C before further manipulation. This reaction time is necessary to obtain full complexation of trypsin with the slow binding inhibitor (Schultz et al., 1989). The remaining excess of free leupeptin was then removed either by ultrafiltration using an Amicon PM10 membrane or by gel filtration using Sephadex G-25. For proton NMR experiments, after the initial 2-h incubation the water was removed by lyophilization, and the trypsin–leupeptin complex was dissolved in 99.98% D_2O. All NMR experiments were recorded at ambient temperature (18–20 °C) in a 5-mm sample tube in 400 μL of D_2O–phosphate buffer. The pH of the solution was adjusted with 0.1 N NaOD or 0.1 N DCl, and the final pH also recorded after acquisition of the NMR data. Titration curves were fitted to the Hill equation by nonlinear least-squares regression analysis.

Samples for solid-state NMR were prepared under conditions similar to those previously described for X-ray crystallography. Solid trypsin (25 mg) was suspended in 3 M ammonium sulfate and 0.1 M phosphate buffer, pH 7.6, containing 5 mM [1-^{13}C]leupeptin for 15 days. The buffer was removed by centrifugation prior to data acquisition. The pH of the trypsin–leupeptin complex was then adjusted to 4 by resuspending the sample in 3 M ammonium sulfate pH 4 for several hours.

NMR Spectroscopy. ^{13}C NMR spectra were recorded at 75.47 MHz on a Bruker WM300 wide bore spectrometer equipped with a 5-mm C/H probe. ^{13}C acquistion parameters employed were 1.0-s repetition delay, 6.0-μs pulse width, 0.5-s acquisition time (16K data points), and low-power (0.25 W) Waltz proton decoupling. ^{1}H NMR spectra were obtained at 500.13 MHz on the Bruker AM500 spectrometer equipped with a home-built "reverse mode" H/C probe, a BSV6 broadband amplifier modified to allow fast power switching on the ^{13}C and ^{1}H transmitters (Tellier et al., 1990), and an Aspect 3000 computer. All proton ^{13}C-edited spectra were recorded with ^{13}C decoupling during acquistion (0.1 s) by using low-power Waltz decoupling (3.2 kHz rf field). The 90° pulse widths were 24 μs; ^{1}H decoupler, 19 μs; ^{13}C high power and 115 μs; ^{13}C low power. The sequence used to obtain selective proton ^{13}C-edited spectra consisted of a conventional spin-echo difference experiment ($90°_H$–τ–$90°_C$–$180°_H$–$90°_C$–τ–acquire) in which the first ^{13}C 90° pulse was substituted by a selective half-Gaussian pulse (Tellier et al., 1990) centered at the frequency of the desired ^{13}C resonance. An equivalent ^{13}C semiselective half-Gaussian pulse is used to convert the 2D heteronuclear multiquantum correlated spectroscopy with NOE relay (HMQC-NOESY) (Gronenborn et al., 1989) to a selective isotope-edited 1D NOESY experiment. A 2.8-ms spin-echo (τ) delay was used in both experiments.

Solid-state CPMAS ^{13}C NMR spectra were recorded at 75.46 MHz on a Bruker MSL-300 spectrometer equipped with an Aspect 3000 computer using a cross polarization contact time of 1 ms, a recycle time of 5 s, and a spinning rate of 3500–4000 Hz.

Results

^{13}C NMR Studies of the Enzyme–Inhibitor Complex. Leupeptin exists in three interconverting forms in equilibrium in aqueous solution (Scheme I), namely, leupeptin hydrate (42%), the cyclic carbinolamine diastereomers (56%) generated by the addition of the guanidino nitrogen to the aldehydic carbon, and the free aldehyde (2%) (Schultz et al., 1989). Consequently, four resonances for the enriched carbon of [1-^{13}C]leupeptin are observed in the ^{13}C NMR spectrum shown in Figure 1A: 202.1 ppm (aldehyde), 90.3 ppm (hy-

[1] Abbreviations: NMR, nuclear magnetic resonance; NOE, nuclear Overhauser effect; 1D NOESY, one-dimensional nuclear Overhauser enhancement spectroscopy; CPMAS, cross-polarization magic-angle spinning.

Scheme I

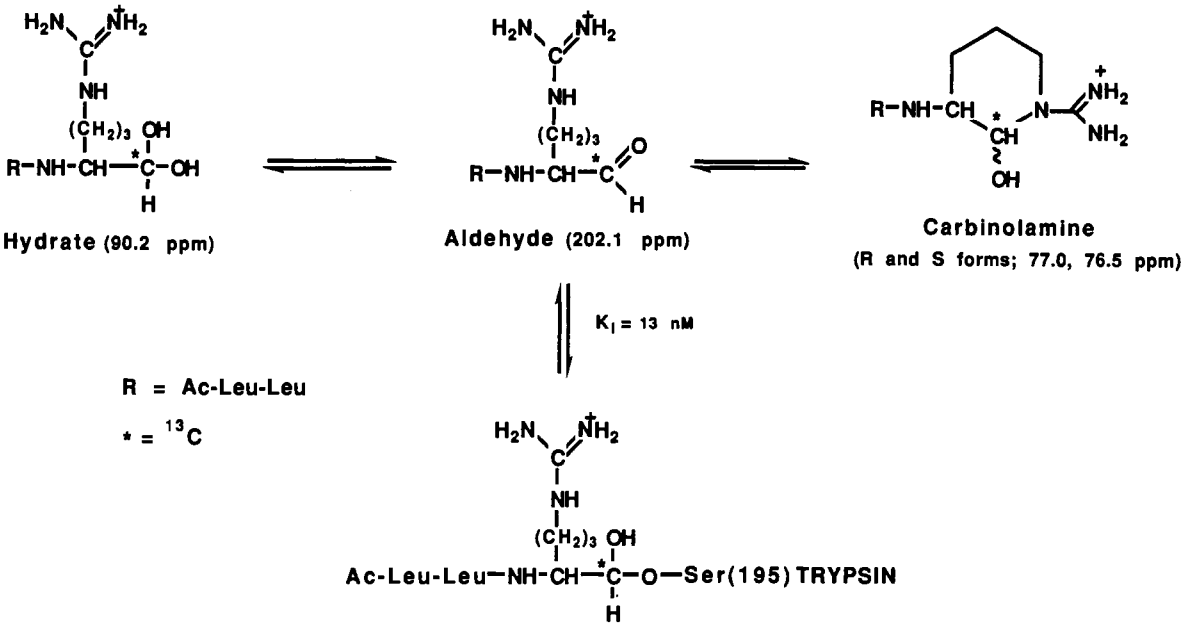

drate), and 76.5 and 77.0 ppm (cyclic carbinolamine, *R* and *S* configurations). In addition, due to the exchange of the slightly acidic argininal α-proton, leupeptin racemizes in aqueous solution, giving rise to a second ^{13}C peak (δ 90.18, not resolved in spectrum shown) attributed to the D-isomer (at arginine) of the hydrate. Incubation of a 2-fold excess of [1-^{13}C]leupeptin with 2 mM trypsin in 0.1 M phosphate buffer, pH 7.6, leads to the complete disappearance of the hydrate signal at 90.3 ppm, confirming trypsin's preference to bind only the L-diastereomer. More importantly, however, is the observation of two new signals at 98.8 and 97.2 ppm (86:14 ratio) (Figure 1B). These new signals display a broad line width (35 Hz) and are still present (Figure 1C,D) after removal of small molecules by filtration (Amicon PM10), indicating a macromolecule-associated signal. By comparison of their chemical shifts to those of a model hemiacetal formed between *N*-benzoyl-L-phenylalaninal and methanol (δ 98.2, unpublished results) and also to previous studies of aldehyde inhibitor–chymotrypsin complexes (Shah et al., 1984), we can assign these new signals to tetrahedral species resulting from the reaction between the aldehyde and the hydroxyl group of the serine residue 195 at the active site.

The effect of pH on the two hemiacetal signals of the [1-^{13}C]leupeptin–trypsin complex was next investigated by ^{13}C NMR spectroscopy. It can be seen from Figure 2 that the chemical shifts for *both* signals are pH dependent. When the pH is lowered from 7.0 to 3.0, the signal at 98.8 ppm moves upfield to 95.5 ppm following a titration curve (●) with a pK_a = 4.69 (Figure 3A) while diminishing in intensity. Although not readily discernable in Figure 2, the signal at 97.2 ppm also follows a titration curve (○) corresponding to a pK_a = 5.67 (Figure 3A), shifting 0.7 ppm upfield at low pH. The amplitudes of the hemiacetal peaks were next plotted as a function of pH, shown in Figure 3B. As illustrated here (and in Figure 2), the intensity of the hemiacetal signal originally at 98.8 ppm rapidly decreases on lowering the pH with a concomitant, although not uniform, increase of the hemiacetal signal initially at 97.2 ppm. Interestingly, the decrease in intensity of the hemiacetal signal at 98.8 ppm (Figure 3B) roughly parallels its titration curve (Figure 3A), suggesting an unfavorable modification of its structure that increases its binding constant

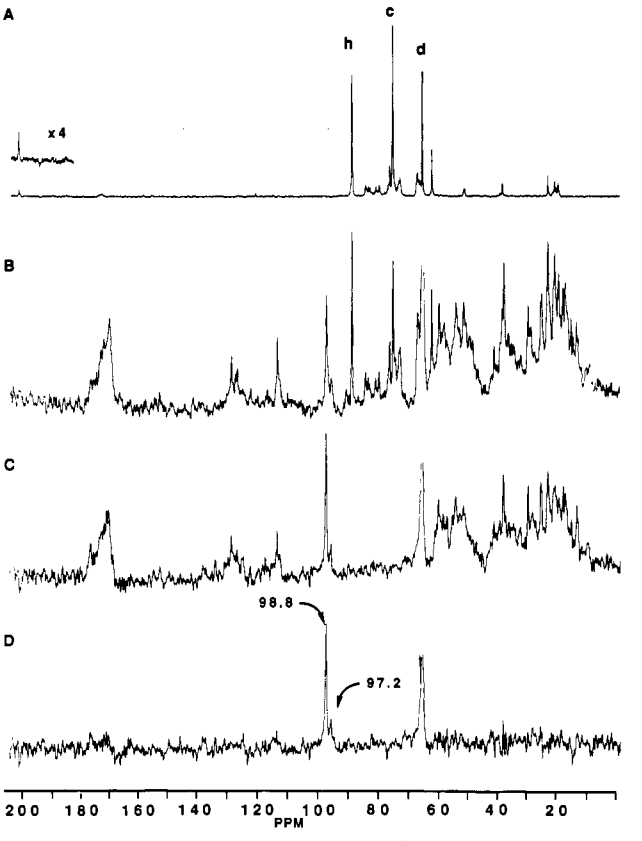

FIGURE 1: Proton-decoupled 75.46 MHz ^{13}C NMR spectra of [1-^{13}C]leupeptin and [1-^{13}C]leupeptin–trypsin complexes in 0.1 M phosphate buffer (pH 7.4) containing 10% D_2O at 20 °C. (A) 4 mM leupeptin, 40 000 scans; (B) 4 mM leupeptin + 2 mM trypsin, 48 000 scans; (C) leupeptin–trypsin complex after filtration through Amicon PM 10 membrane, 48 000 scans; (D) difference spectrum (C minus 2 mM trypsin control, not shown). Signal assignments: (h) leupeptin hydrate, (c) carbinolamine, and (d) dioxane. The majority of the remaining signals in spectrum A can be attributed to the natural abundance carbons of leupeptin.

at lower pH. In addition, the rapid appearance of a third resonance assignable to the hydrate form (90.3 ppm, Figure 2) is noted below pH 5, indicating dissociation of the complex

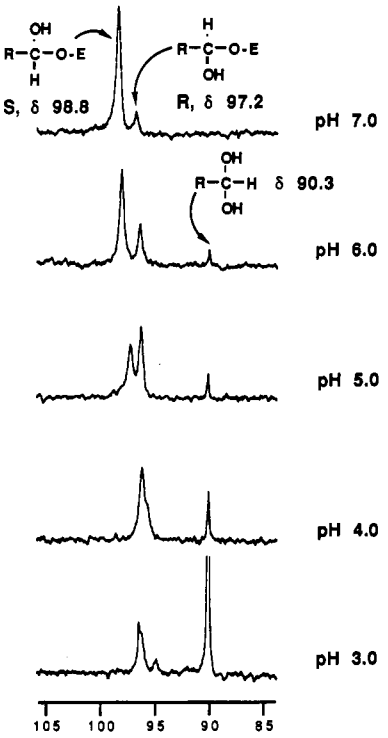

FIGURE 2: Hemiacetal region of the 75.46 MHz ^{13}C NMR spectra of the [1-^{13}C]leupeptin–trypsin complex, prepared as in Figure 2C. Each spectrum was obtained on the same sample with 40 000 scans, at the pH values listed. (Stereochemical assignments shown are from subsequent NOE experiments.)

related to the known increase in leupeptin's dissociation constant (K_d) at low pH (Kuramochi et al., 1979). The reversibility of the process is demonstrated by reequilibration of the sample from pH 3.0 to 7.0, during which the original signal intensities and chemical shifts are restored. These results clearly demonstrate that trypsin binds covalently to the leupeptin inhibitor in two pH-dependent interconverting tetrahedral forms.

^1H-Detected ^{13}C-Edited NMR Studies. Isotope-edited techniques (Griffey & Redfield, 1987; Bax & Weiss, 1987; Fesik et al., 1988) were next used to identify the hemiacetal protons and their environment in the active site of trypsin. These powerful new pulse sequences take advantage of the isotopic enrichment at the hemiacetal carbon, allowing for the suppression all remaining protons attached to ^{12}C that would otherwise prevent the observation of the hemiacetal signal.

Figure 4 shows the proton ^{13}C-edited spectra of the [1-^{13}C]leupeptin–trypsin complex at different pH's. In the standard nonselective ^1H isotope-edited spectrum (Figure 4A), the signals in the 4.8–5.5 ppm region come mainly from free leupeptin and are due to the hydrate (δ 4.98) and to the cyclic carbinolamine form (δ 5.32, 5.41) (Schultz et al., 1989). By use of a selective ^{13}C-edited sequence, only the hemiacetal proton of the bound leupeptin was observed (Figure 4B) by selective excitation at the corresponding ^{13}C chemical shift (98.8 ppm). The observed chemical shift (δ 4.96) is in good agreement with that predicted for a hemiacetal proton; however, at pH 7 the peak is nearly coincident with that of the free hydrate. The hemiacetal assignment was subsequently confirmed in a separate experiment in which the excess leupeptin was removed by filtration (data not shown). The chemical shifts of leupeptin at pH 7 are summarized in Table I.

The pH dependency of the hemiacetal proton signal was next investigated by using the nonselective pulse sequence to

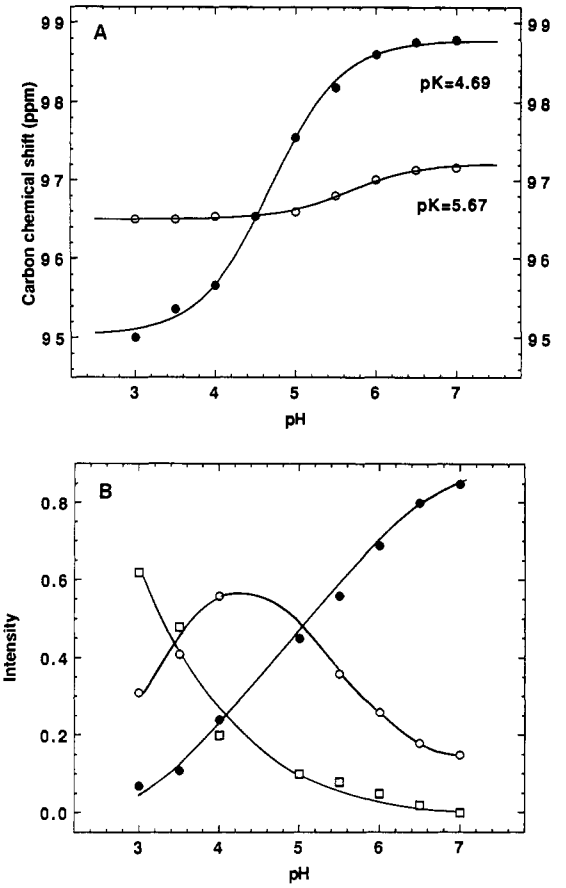

FIGURE 3: pH dependence of ^{13}C chemical shift and intensity of the two hemiacetals in the leupeptin–trypsin complex shown in Figure 2. In both plots, curves ● and ○ represents the chemical shift or intensity corresponding to the hemiacetal peaks originally observed at 98.8 and 97.2 ppm at pH 7.4. The pK_a values shown in plot A were obtained by a nonlinear least-squares fit of the data to the Hill equation. Curve □ in plot B represents the intensity of the hydrate at 90.3 ppm.

Table I: Carbon and Proton Assignments of Free and Bound Leupeptin at the ^{13}C-Enriched Position at pH 7

chemical form	chemical shift[a] (ppm)		
	^{13}C	$\omega_{1/2}$ (Hz)	^1H
aldehyde	202.1	15 (±2)	9.32
hydrate	90.2	22 (±2)	4.98
carbinolamine	76.5	15 (±2)	5.41
R and *S* forms	77.5	15 (±2)	5.32
hemiacetal (*S*)	98.8	35–40 (±4)	4.96
hemiacetal (*R*)	97.2	40 (±4)	5.28

[a] Chemical shifts are reported with respect to dioxane (66.5 ppm) for carbon and to trimethylsilanepropionic acid-d_5 (0.0 ppm) for proton.

avoid unequal excitation of the hemiacetal carbons. When the pH is lowered, the hemiacetal proton moves downfield, following a curve similar to the titration curve of the high pH (δ 98.8) hemiacetal carbon observed by ^{13}C NMR. As with the ^{13}C NMR experiment, the titration of the hemiacetal proton is also accompanied by a reduction of its peak intensity and the appearance of a second proton signal at 5.24 ppm (Figure 4C,D), confirming the existence of two different interconverting hemiacetal complexes of leupeptin with trypsin.

To determine the immediate environment of the hemiacetal proton, selective ^{13}C-edited 1D NOESY experiments were next performed. This technique combines the through-space connectivity of an NOE experiment with the simplification afforded by the selective ^{13}C-edited sequence allowing for rapid acquisition of simple NOE spectra (<3 h). Figure 5A displays

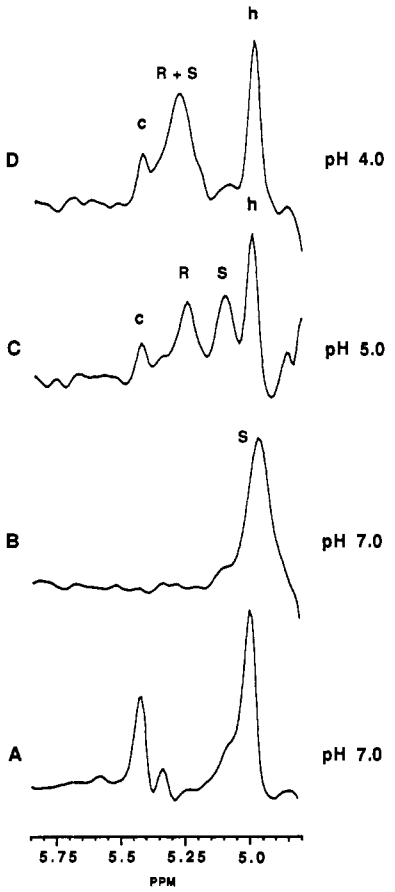

FIGURE 4: 500.13 MHz proton ^{13}C-edited spectra of the [1-^{13}C]-leupeptin–trypsin complex in 0.1 M phosphate D_2O buffer at pH's indicated. Spectra A, C, and D were obtained in 1028 scans by using the nonselective sequence, while spectrum B was obtained by using the selective Guassian pulse. Signal assignments: (c) carbinolamine; (h) hydrate; *R* and *S*, hemiacetal protons (stereochemistry as defined by subsequent NOE experiments).

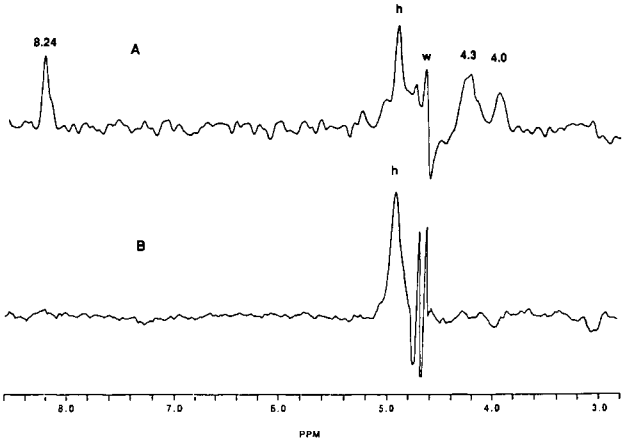

FIGURE 5: 500.13 MHz proton spectra of the [^{13}C]leupeptin–trypsin complex in D_2O phosphate buffer, pH 7.4. (A) Selective 1D NOESY spectrum obtained with a 100-ms mixing time showing new signals at 8.24, 4.3, and 4.0 ppm. Peak w is assigned to residual water. (B) Selective proton ^{13}C-edited spectrum showing the hemiacetal signal (h) at 4.96 ppm. Both spectra A and B were recorded with 10240 scans.

the isotope-edited NOE spectrum obtained on the leupeptin–trypsin complex at pH 7. In contrast to the normal selective proton-edited spectrum (Figure 5B), three NOE peaks at 8.24, 4.3, and 4.0 ppm are clearly seen which correspond to protons that are close in space to the hemiacetal proton. The resonance at 8.24 ppm could correspond to either an unexchanged amide

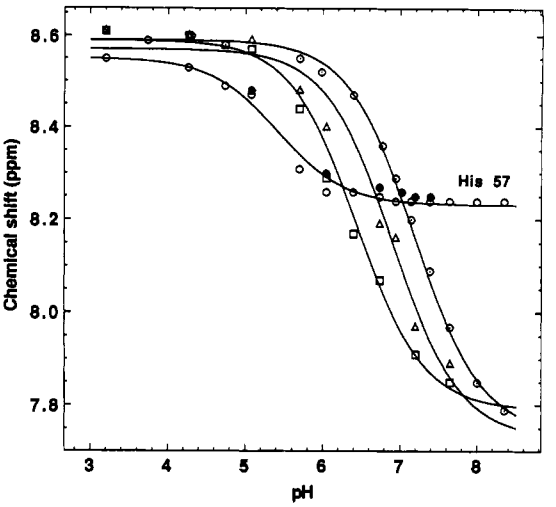

FIGURE 6: ^1H NMR titration curves (at 500 MHz) of the histidyl C2 protons of the [^{13}C]leupeptin–trypsin complex. The titration curves yield pK_a values of 7.19 (⊙), 6.91 (△), 6.44 (□), and 5.42 (○) for the four histidines. The titration curve of the NOE peak obtained in the selective edited 1D NOESY experiment is also reported (●).

Table II: Active Site Protons Residing Less Than 3.8 Å from the Hemiacetal Proton in the Leupeptin–Trypsin Complex at pH 7

residues[a]	X-ray data distance (Å)	NOE data chemical shift	NOE data distance (Å)
Arg (leupeptin)			
CαH	2.03		
CβH1	2.81		
CβH2	3.61		
Ser 195			
CβH1	2.74	4.30	2.77[b]
CβH2	3.50	4.00	3.37[c]
His 57			
NεH		8.25	2.96[b]

[a] Only the nonexchangable protons are tabulated. [b] The NOE distance was derived from the cross-relaxation rate σ_{ij} (see the text). [c] Calculated by using the previously determined distances as an internal reference and the equation $N_{ij}(t)/N_{ik}(t) = (r_{ik}/r_{ij})^6$ where $N(t)$ is the amplitude of the NOE peak for a mixing time t.

proton or to a histidine C2 proton. However, in our experiments the samples are fully exchanged with D_2O so that most of the amide protons are replaced by deuterium. The possibility of the presence of a nonexchangeable amide proton inside the active site is unlikely since the active site is accessible to water and the leupeptin inhibition is reversible. To confirm the histidine assignment, we next studied the titration curve of the four histidine C2 protons in the leupeptin–trypsin complex by the standard proton spin-echo sequence described previously (Campbell et al., 1975). The data are reported in Figure 6 and show that three histidines titrate normally with pK_a's between 6.4 and 7.2. The fourth histidine (○, Figure 6), previously assigned as the active site His57 (Markley & Porubcan, 1976), exhibits the same chemical shift (8.25 ppm) as the signal observed in the 1D NOE experiment at pH 7. Furthermore, the NOE signal was observed at different pHs, and its chemical shift (●) is recorded on the histidine titration curve (Figure 6). It can be seen that the values fit the His57 titration curve exactly above pH 5. Below pH 5, the NOE signal disappears as the observed hemiacetal is converted to the low pH form. The data clearly demonstrate that the NOE peak at 8.24 ppm corresponds to the C2 proton of His57.

Two other NOE peaks at 4.3 and 4.0 ppm (Figure 5A) are observed at pH 7 and can be tentatively assigned by inspection of the active site model of the leupeptin–trypsin complex de-

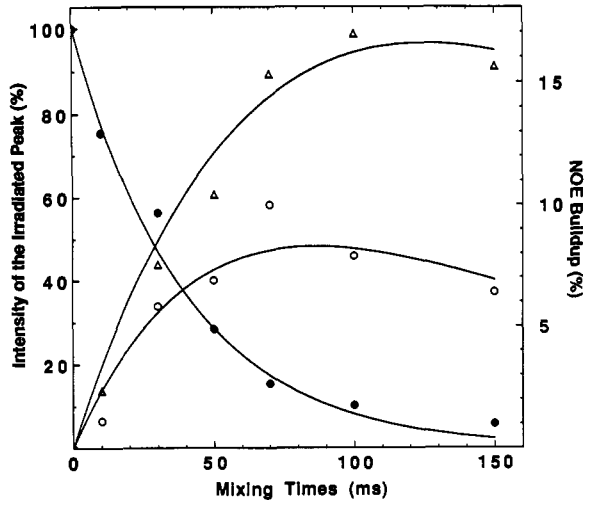

FIGURE 7: NOE buildup obtained with the selective 1D NOESY experiment on the [^{13}C]leupeptin–trypsin complex. The mixing time (τ_m) was incremented as indicated in the figure. Decay of the intensity of the hemiacetal proton at 4.96 ppm (●); buildup of the NOE effect on the peaks at 8.25 (△) and 4.3 ppm (○).

rived by fitting leupeptin into X-ray crystal structure of trypsin available from the protein data bank. Table II lists the proton chemical shifts of all residues that are within 4 Å of the hemiacetal proton. The closest protons that could account for the NOE observed at 4.3 and 4.0 ppm are the β-protons of Ser195. The arginine α-proton of leupeptin would give a similar chemical shift, but it exchanges rapidly with deuterium (within 1 h) and therefore would not give an NOE peak. The chemical shift range of the β-protons of serine (3.7–4.5 ppm) in a previously assigned protein (Chazin & Wright, 1988) is in accord with our NOE peak assignments.

An the cross-relaxation rates between protons are proportional to r^{-6}, the amplitude of an NOE peak provides a sensitive measure of proton–proton distances. The cross-relaxation rate (σ_{ij}) between protons i and j can be derived from the NOE buildup curve from which, at short mixing times (τ_m), the intensity of the NOE peak (A_{ij}) is given by the approximation $A_{ij}\tau_m \sim \sigma_{ij}\tau_m$ (Noggle & Schirmer, 1971). Figure 7 shows the two NOE buildup curves corresponding to the resonances at 8.24 and 4.3 ppm as well as the decrease of intensity of the hemiacetal proton as a function of the mixing time. Cross-relaxation rates derived from these curves can be used to calculate the approximate interproton distances (r_{ij}) from

$$\sigma_{ij} = \gamma^4\hbar^2/40\pi^2 r_{ij}^{-6}[6\tau_c/(1 + 4\omega^2\tau_c^2) - \tau_c]$$

assuming a correlation time of the interproton vector (τ_c) equal to the tumbling rate of the whole protein. For the above calculations, a correlation time of 1.70×10^{-8} s was used, estimated from the ^{13}C line width of the hemiacetal resonance (Malthouse, 1988). The interproton distances calculated from the NOE buildup curves are given in Table II.

Finally, while the low intensity of the proton resonance corresponding to the second hemiacetal form at pH <5 precludes measurement of reliable NOE data, a weak NOE signal at 4.2 ppm could be detected (data not shown) that again may originate from one of the β-protons of Ser195.

CPMAS ^{13}C NMR Studies. The CPMAS solid-state NMR spectrum of the complex recorded in high salt concentration at pH 7 (Figure 8A) exhibited very similar chemical shifts (*S*, δ 98.8; *R*, δ 96.5) to those obtained in solution. Although the *S*-isomer again predominates at high pH, a minor increase (from 16 to 33%) of the *R*-isomer was observed. Acquisition of the solid-state spectrum at pH 4 (Figure 8B) also duplicated the solution data, the signal for the *R*-isomer at δ 96.5 predominating. Interestingly, formation of the hydrate at low pH is not observed by CPMAS, indicating a change in the dissociation constant of the complex in the solid state.

Discussion

The mechanism of action of the naturally occurring protease inhibitor leupeptin has been postulated to involve the direct nucleophilic attack of the active site serine hydroxyl group upon the aldehyde of the peptide, resulting in the formation of a stable enzyme–inhibitor complex. In this study, we offer conclusive evidence using NMR spectroscopy that leupeptin forms not one, but two stable hemiacetal complexes, via covalent addition of the hydroxyl group of Ser195 in the active site of trypsin.

Addition of leupeptin, specifically ^{13}C labeled at the aldehyde carbon, to a solution of trypsin at pH 7.6 resulted in the observation of two new ^{13}C NMR signals at 98.8 and 97.2 ppm, the chemical shifts fully consistent with the formation of hemiacetal complexes with the serine hydroxyl of trypsin. The complexes are shown to be sensitive to pH; the signal at 98.8 ppm moves upfield to 95.5 ppm on lowering the pH from 7.6 to 3.0, following the titration curve with a pK_a = 4.69 (Figure 3A), while the peak at δ 97.2 (pH 7.6) experiences a more subtle titration corresponding to a pK_a = 5.67. In addition, while the signal at 98.8 ppm predominates at high pH (>7), its intensity decreases on lowering the pH of the solution, giving rise to a preponderance of the second complex by pH 5, prior to substantial dissociation of both complexes at pH 3. These results, along with the analogous experiment of observing the hemiacetal proton via the selective ^{13}C-edited techniques, suggests the pH-dependent formation of *R* and *S* diastereomeric hemiacetal complexes, interconvertible through the Michaelis complex of leupeptin by attack of Ser195 on either face of the aldehyde.

Structure of the Hemiacetal Complex at High pH. The 1D NOESY experiments described above demonstrate that at pH 7 the hemiacetal proton is within 3.5 Å of the imidazole ring of the His57. With a model derived from available X-ray structures of several trypsin–inhibitor complexes, this constraint implies that the hemiacetal oxygen points toward the oxyanion hole, resulting in the *S* configuration about the hemiacetal carbon. Employing local distance constraints imposed by the NOE results, a computer graphic model was constructed by using the geometry optimization routine. As illustrated in Figure 9A, the model predicts the close proximity of the hemiacetal proton to both the C2 proton of His57 and the β-protons of Ser195 and indicates that the hemiacetal oxygen resides in the oxyanion hole, within hydrogen-bonding distance of the backbone amides of Gly193 and Ser195. For comparison, the alternate structure corresponding to the *R* configuration was also modeled (Figure 9B) and suggests the formation of a hydrogen bond between the hemiacetal oxygen and ε-nitrogen of His57. Inspection of both *R* and *S* models shows that the binding of either diastereomer does not require extended modification inside the active site or in the inhibitor configuration, except for a small tilt in the imidazole ring of His57. The observation of both *R* and *S* forms of the leupeptin inhibitor complex by NMR is in accord with previous X-ray studies on the chymostatin complex of *Streptomyces griseus* protease A (Delbaere & Brayer, 1985) where *both* anomeric configurations were observed at pH 4.1.[2] Thus, the two

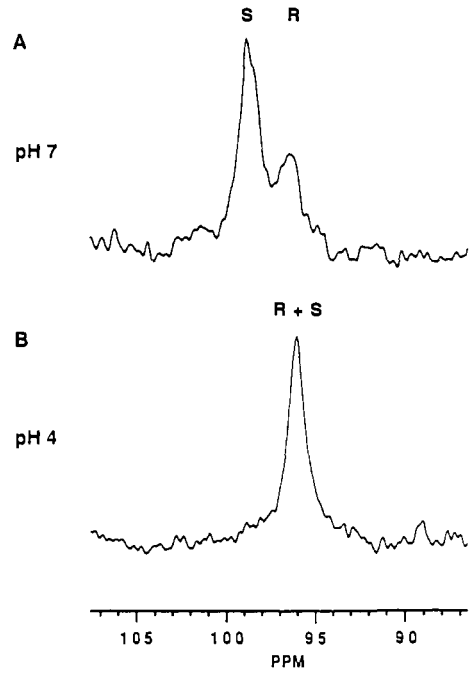

FIGURE 8: 75.4 MHz CPMAS ^{13}C NMR spectra of the trypsin–leupeptin complex after soaking commercial trypsin crystals for 15 days with 5 mM [^{13}C]leupeptin in 3 M ammonium sulfate and 0.1 M phosphate buffer at pH 7, then at pH 4. Each spectrum represents 15 000 scans.

hemiacetal signals observed by NMR originate from the slowly interconverting diastereomeric *R* and *S* complexes, with a preference for the *S* configuration at pH >5. Shah et al. (1984) also noted two pH-dependent ^{13}C NMR signals for the complex of [1-^{13}C]-*N*-acetyl-L-phenylalaninal with chymotrypsin.

Furthermore, our CPMAS ^{13}C NMR data (Figure 8) confirm that both diastereomers are indeed present in the solid state and experience a similar pH dependency as their solution-state counterparts. In this regard, it would be of great interest to study the high-resolution X-ray diffraction data for the trypsin–leupeptin complex at both high and low pH, since the solid-state NMR spectrum provides a welcome bridge between the solution NMR data and the structure derived by X-ray crystallography.

Protonation State of the Residues Inside the Active Site. From the foregoing proton NMR studies, it can be concluded that the predominant form of the complex at pH 7 has the *S* configuration in which the hemiacetal oxygen is pointing toward the oxyanion hole. This hemiacetal exhibits large ^{13}C and ^{1}H chemical shift variation on lowering the pH with a pK_a = 4.67 (Figure 3A). The magnitude of ^{13}C chemical shift ($\Delta\delta$ = 3.9 ppm) is too large to be from neighboring ionizable groups (i.e., Asp102 or His57); however, it is consistent with *direct* oxygen hemiacetal or hemiketal titrations (Malthouse et al., 1985; Liang & Abeles, 1987). This suggests that the observed titration is due to protonation of the hemiacetal oxygen, although the pK_a is about 7 units lower than the value of 11 calculated from free energy predictions (Fastrez, 1977) or measured on model compounds. The observation provides a direct demonstration of the high ability of the oxyanion hole to stabilize an oxyanion of the tetrahedral adduct. Even lower pK_a values (~3) have been found for a peptidyl trifluoromethyl ketone inhibitor (Brady et al., 1989). A smaller but still substantial decrease of the pK_a (to ~8) of the hemiketal hydroxyl has also been reported in the complex formed between trypsin and *N*-CBZ-lysyl chloromethyl ketone (Malthouse et al., 1985).

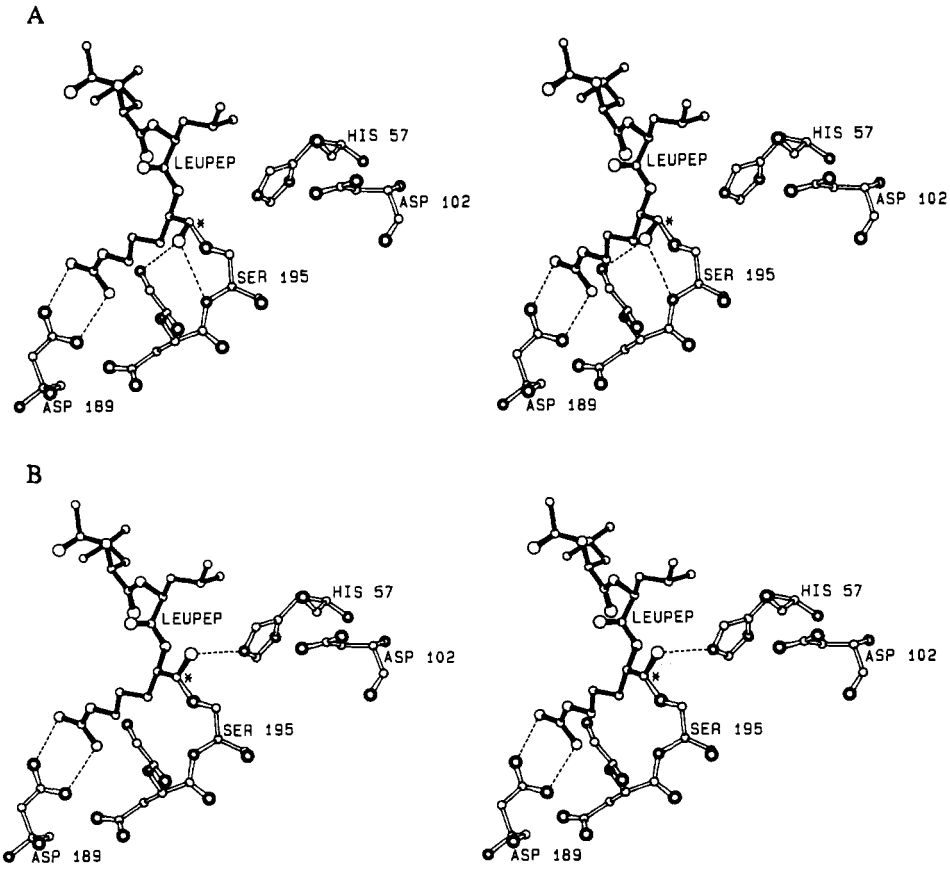

FIGURE 9: Stereo structures of the two diastereomers of the leupeptin–trypsin complex showing the hemiacetal in the (A) *S* configuration and (B) the *R* configuration. Bonds of the inhibitor are filled. Hydrogen bonds are shown as dashed lines.

Experimental evidence also supports the assignment of the *R*-diastereomer to the hemiacetal favored at low pH. The small chemical shift observed for titration of this species ($\Delta\delta$ = 0.7 ppm) is consistent with titration of a neighboring functional group, and moreover its pK_a (5.67) is strikingly similar to that observed for the C2 proton of His57 (Figure 6). The proton NMR results also suggest that the imidazole ring of the histidine remains at least partially protonated in the complex over the pH range 3–8.5, as judged by the value of the chemical shift. The raising of the histidine pK_a upon inhibitor binding seems to be a common feature of all serine proteases and a necessary step in the stabilization of the tetrahedral adduct (Porubcan et al., 1979; Primrose et al., 1985). However, a small variation of the chemical shift is observed for His57 with a p$K_a \sim 5.6$ allowing the histidine to reach a chemical shift normally found for a fully protonated histidine, suggesting that this small titration observed could be due to protonation of Asp102. Hence the *R* diastereomer, depicted to share a hydrogen bond via the hemiacetal hydroxyl and Nϵ of His57 (Figure 9B), may be sensing the protonation at Asp 102. The increase in pK_a of the Asp102 is not well understood but could be correlated with the increase in pK_a of His57. However, the residue (Asp102) seems to be important in stabilizing the anionic transition-state analogue, in support of the theoretical considerations of Warshel et al. (1989) on the role of electrostatic interactions in the catalytic mechanism of serine proteases.

Relevance of Two Different Hemiacetal Complexes for the Catalytic Mechanism of Serine Proteases. This study has shown that peptide aldehydes can form isomeric hemiacetal adducts with Ser195 of trypsin. The question now arises as to whether two pH-dependent diastereomeric tetrahedral intermediates could be involved in the catalytic mechanism of the serine proteases. In principle, the presence of the leaving group (–NHR) in the first tetrahedral intermediate should disfavor the configuration in which the oxyanion is pointed toward His57 due to steric hindrance within the oxyanion hole, limiting catalysis to a *S*-configured mechanism. In the case of simple esters, however, the results imply that at low pH trypsin could also function via the *R*-configured tetrahedral intermediate through formation of a hydrogen bond between the imidazole ring of His57 and the tetrahedral hydroxyl. Additionally, the ability of trypsin to bind either hemiacetal configuration of the first tetrahedral adduct suggests that the same hydrogen-bonding arrangement would be important in stabilizing the second tetrahedral adduct (where a water molecule has been added to the acyl–enzyme intermediate) that has one oxygen atom in the oxyanion hole *and* one participating in hydrogen bonding to His57.

In summary, we have demonstrated that ^{13}C-edited ^{1}H chemical shift and NOE experiments provide detailed information about the nature of higher molecular weight enzyme–inhibitor complexes, leading to a model of the inhibitor within the active site pocket via structural information on the protonation state of the residues and on the absolute stereochemistry of two tetrahedral adducts. This approach provides a dynamic view of the molecular events taking place at the active site as a function of pH and should complement crystallographic studies of the leupeptin–trypsin complex, currently in progress.[2]

[2] A preliminary X-ray crystal structure of the leupeptin–trypsin complex reveals the noncovalent binding of the leupeptin backbone to trypsin as well as the covalent interaction of Ser195 with the hemiacetal carbon (Meyer et al., unpublished results). However, the high temperature coefficient for the electron density at the hemiacetal carbon leads to a structural dilemma since the "average" geometry at this carbon appears to be *planar*. Such "sp^2" hybridization about the hemiacetal carbon could be rationalized, in complete accord with the NMR experiments, by invoking the existence of both *R* and *S* tetrahedral forms in the crystal lattice, producing a time-averaged hemiacetal structure with the resultant planar geometry.

Acknowledgments

We thak Dr. E. F. Meyer, Jr. (Biochemistry Department, Texas A&M University) for information concerning the preliminary X-ray structure of the leupeptin–trypsin complex and Dr. P.-J. Chu for technical assistance with solid-state NMR experiments.

References

Aoyagi, T., Takeuchi, T., Matsuzaki, A., Kawamura, K., Kondo, S., Hamada, M., Maeda, K., & Umezawa, H. (1969) *J. Antibiot. 22*, 283–286.

Bajusz, S., Szell, H. E., Bagdy, D., Barabas, E., Dioszegi, M., Fittler, Z., Jozsa, F., Horvath, G., & Tomori, J. E. European Patent Application EP 185390, 1986.

Bax, A., & Weiss, M. A. (1987) *J. Magn. Reson. 71*, 571–575.

Borin, G., Gavino, C., Giafranco, C., Marchiori, F., & Müller-Esterl, W. (1981) *Hoppe-Seyler's Z. Physiol. Chem. 362*, 1435–1445.

Brady, K., Liang, T. C., & Abeles, R. H. (1989) *Biochemistry 28*, 9066–9070.

Campbell, I. D., Dobson, C. M., Williams, R. J. P., & Wright, P. E. (1975) *FEBS Lett. 57*, 96–99.

Chazin, W. J., Rance, M., & Wright, P. E. (1988) *J. Mol. Biol. 202*, 603–622.

Chen. R., Gorenstein, D. G., Kennedy, W. P., Lowe, G., Nurse, D., & Schultz, R. M. (1979) *Biochemistry 18*, 921–926.

Delbaere, L. T. J., & Brayer, G. D. J. (1985) *J. Mol. Biol. 183*, 89–103.

Fastrez, J. (1977) *J. Am. Chem. Soc. 99*, 7004–7013.

Fesik, S. W., Luly, J. R., Erickson, J. W., & Abad-Zapatero, C. A. (1988) *Biochemistry 22*, 8291–8301.

Griffey, R. H., & Redfield, A. G. (1987) *Q. Rev. Biophys. 19*, 51–82.

Gronenborn, A. M., Bax, A., Wingfield, P. T., & Clore, G. M. (1989) *FEBS Lett. 243*, 93–98.

Hunkapiller, M. W., Smallcombe, S. H., Whitaker, D. R., & Richards, J. H. (1973) *Biochemistry 12*, 4732–4743.

Kennedy, W. P., & Schultz, R. M. (1979) *Biochemistry 18*, 349–356.

Kuramochi, H., Nakata, H., & Ishii, S. (1979) *J. Biochem. (Tokyo) 86*, 1403–1410.

Liang, T. C., & Abeles, R. H. (1987) *Biochemistry 26*, 7603–7608.

Mackenzie, N. E., Grant, S. K., Scott, A. I., & Malthouse, J. P. G. (1986) *Biochemistry 25*, 2293–2298.

Malthouse, J. P. G., Primrose, W. U., Mackenzie, N. E., & Scott, A. I. (1985) *Biochemistry 24*, 3478–3487.

Markley, J. L., & Porubcan, M. A. (1976) *J. Mol. Biol. 102*, 487–509.

Naithani, V. K., & Gattner, H. (1981) *Hoppe-Seyler's Z. Physiol. Chem. 362*, 685–695.

Noggle, J. H., & Schirmer, R. E. (1971) *The Nuclear Overhauser Effect*, Academic Press, New York.

Ortiz, C. (1990) Ph.D. Dissertation, Texas A&M University.

Pauling, L. (1946) *Chem. Eng. News 263*, 294–297.

Porubcan, M. A., Westler, W. M., & Markley, J. L. (1979) *Biochemistry 18*, 4108–4116.

Primrose, W. U., Scott, A. I., Mackenzie, N. E., & Malthouse, J. P. G. (1985) *Biochem. J. 231*, 677–682.

Schultz, R. M., Varma-Nelson, P., Ortiz, R., Kozlovski, A., Orawski, A. T., Pagast, P., & Frankfater, A. J. (1989) *J. Biol. Chem. 264*, 1497–1507.
Shah, D. O., & Gorenstein, D. G. (1983) *Biochemistry 22*, 6096–6101.
Shah, D. O., Lai, K., & Gorenstein, D. G. (1984) *J. Am. Chem. Soc. 106*, 4272–4273.
Smith, S. O., Farr-Jones, S., Griffin, R. G., & Bachovchin, W. W. (1989) *Science 244*, 961–964.
Tellier, C., Williams, H., Gao, Y., Ortiz, C., Stolowich, N. J., & Scott, A. I. (1990) *J. Magn. Reson. 90*, 600–605.
Thompson, R. (1973) *Biochemistry 12*, 47–51.
Warshel, A., Naray-Szabo, G., Sussman, F., & Hwang, J. K. (1989) *Biochemistry 28*, 3629–3637.

A Monolayer and Bulk Study on the Kinetic Behavior of *Pseudomonas glumae* Lipase Using Synthetic Pseudoglycerides†

Annemieke M. Th. J. Deveer,*,‡ Ruud Dijkman,‡ Marijke Leuveling-Tjeenk,‡ Lambertus van den Berg,‡ Stephane Ransac,§ Max Batenburg,∥ Maarten Egmond,∥ Hubertus M. Verheij,‡ and Gerard H. de Haas‡

Department for Enzymology and Protein Engineering, CBLE, Trans III, Padualaan 8, 3584 CH Utrecht, The Netherlands, Centre de Biochimie et Biologie Moleculaire, CNRS, 31 Chemin Joseph Aiguier, 13402, Marseille Cedex 9, France, and Unilever Research Laboratory, Postbus 114, 3130 AC Vlaardingen, The Netherlands

Received May 29, 1991; Revised Manuscript Received July 19, 1991

ABSTRACT: A heat-stable lipase from *Pseudomonas glumae* was purified to homogeneity. Its positional and stereospecific properties were investigated and compared with those of the well-known porcine pancreatic lipase. The kinetic properties of both enzymes were determined by use of six isomeric synthetic pseudoglycerides all composed of a single hydrolyzable fatty acyl ester bond and two lipase-resistant groups: one acylamino and one ether function. Two enzyme assay techniques were applied: a detergent-free system, the monomolecular surface film technique, and the pH-stat technique using clear micellar solutions of substrate in the presence of Triton X-100. Regarding the cleavage of primary ester bonds, *P. glumae* lipase possesses no stereopreference. In contrast, a large stereopreference in favor of the R-isomer is found for the hydrolysis of secondary ester bonds. Secondary ester bonds are efficiently cleaved by the lipase, which makes it of potential interest for enzymatic synthetic purposes. For the hydrolysis of this R-isomer a correlation between the experimental catalytic turnover rate and the binding constant for micelles was observed. The kinetic data of *P. glumae* lipase have been analyzed in terms of the scooting and hopping models for the action of lipolytic enzymes [Upreti, G. C., & Jain, M. K. (1980) *J. Membr. Biol. 55*, 113–121]. The results presented in this study are best explained by assuming that *glumae* lipase leaves the interface after a limited number of catalytic cycles.

Lipases are known as extremely versatile enzymes. Their properties allow widespread application in industry, ranging from (stereo)specific synthesis of compounds (e.g., of interest to the chemical and pharmaceutical business) to the improvement of detergency in laundry washing systems. For optimal application of lipases it is important, however, to understand their basic properties, e.g., the recognition of lipid–water interfaces. This understanding can be used to adjust the properties of the applied lipase with genetic engineering techniques. Structural information of lipases is generally rather poor. Recently, the results of X-ray crystallographic studies on three lipases have appeared in the literature (Brady et al., 1990; Winkler et al., 1990; Schrag et al., 1991) and the structure of a lipase–inhibitor complex has been published (Brzozowski et al., 1991). Only the Cα coordinates of the *Rhizomucor miehei* lipase have recently been deposited in the protein databank. Their homology at the level of amino acid sequence is rather poor, which is a general property of the lipase family.

We have chosen to investigate lipases from *Pseudomonas* species, with one reason being their preferred properties in several application areas like laundry systems and in the transesterification of edible fats, as well as extensive sequence information of *Pseudomonas* lipases that are at least 90% homologous. The lipase from *Pseudomonas glumae* is a 32-kDa protein that consists of a single chain. The enzyme is not glycosylated and contains one disulfide bridge between residues 190 and 269. The existence of one consensus peptide is found in the amino acid sequence surrounding serine 87: G-X-S-X-G. This sequence is encountered in many other lipases and proteases (Brenner et al., 1988) and is shown to be present at the active site of these enzymes.

The determination of the positional and stereospecific preference of lipases acting on natural or synthetic triglycerides is subject to several problems. In theory, enantiomeric triglycerides containing three different acyl groups seem to be ideal substrates for the investigation of the properties of lipases. The enzymatically released free fatty acids can be separated

† This research was carried out with the financial support of the Bridge Programme of the European Economic Community and fellowship support was obtained from Unilever Research Laboratory, Vlaardingen.
* Address correspondence to this author at Unilever Research Laboratory, Postbus 114, 3130 AC, Vlaardingen, The Netherlands.
‡ Department for Enzymology and Protein Engineering.
§ Centre de Biochimie et Biologie Moleculaire.
∥ Unilever Research Laboratory.

0006-2960/91/0430-10034$02.50/0